MRI Signal Formation: From Spins to Measured Signal

Bernd Müller-Bierl

April 2026

Contents

1 Introduction **2**

2 Nuclear Spins and the Rotating Frame **2**
2.1 Nuclear Spins and Precession 2
2.2 RF Excitation and Transverse Magnetization 4

3 Signal and Echo Formation **4**
3.1 Signal Formation and Dephasing 4
3.2 Echo Formation (Spin Echo, Gradient Echo) 6

4 Relaxation and Contrast (T_1, T_2, T_2^*) **7**

5 Basic Sequences (SE, GRE) **10**
5.1 Spin Echo (SE) 10
5.2 Gradient Echo (GRE) 11
5.3 Gradient-Echo vs. Spin-Echo Imaging 12

6 Beyond Basic Sequences **13**
6.1 Steady-State Imaging (SSFP) 13
6.2 Ultra-Fast Imaging: Echo Planar Imaging (EPI) 14

7 Spatial Encoding **18**
7.1 Spatial Encoding (Conceptual) 18
7.2 Spatial Encoding (Mathematical Formulation) 21

8 Lung MRI: Acquisition and Functional Imaging **21**
8.1 Acquisition Strategies: Example of FLORET 22
8.2 Functional Imaging Without Contrast: Example of PREFUL 23

9 Conclusion and Outlook **24**

References **25**

---

1 Introduction

Magnetic resonance imaging (MRI) is a versatile and powerful imaging modality that provides detailed insight into the structure and function of biological tissue. Unlike many other imaging techniques, MRI does not rely on ionizing radiation, but instead exploits the interaction between nuclear spins and externally applied magnetic fields.

Despite its widespread clinical use, the underlying principles of MRI are often perceived as complex, as they involve concepts from quantum mechanics, electromagnetism, and signal processing. In particular, the relation between the measured signal and the resulting image is not immediately intuitive, since spatial information is not acquired directly, but encoded in the phase and frequency of the signal.

The aim of this document is to provide a coherent and physically grounded introduction to the fundamentals of MRI. Starting from the behavior of nuclear spins in a magnetic field, the mechanisms of signal generation, relaxation, and echo formation are developed step by step. Building on this foundation, common pulse sequences and modern fast imaging techniques are introduced.

A central objective is to establish a clear understanding of spatial encoding and the concept of k-space. By linking physical intuition with a quantitative description, the reconstruction of images from measured signals is presented as a natural consequence of the underlying physics.

The presentation follows a structured progression from basic principles to more advanced imaging strategies, with the goal of making MRI both conceptually transparent and mathematically accessible.

Motivation and Perspective

Magnetic resonance imaging is often introduced as a sequence of established concepts, ranging from spin dynamics to image reconstruction. However, in many modern applications, particularly in lung imaging, functional MRI, and real-time acquisition, the traditional separation between physical principles, sequence design, and reconstruction becomes increasingly insufficient.

The present document is therefore not intended as a purely descriptive overview, but as a model-based perspective on MRI signal formation, in which the measured signal is understood as the direct consequence of controlled spin dynamics in time-dependent electromagnetic fields.

This viewpoint becomes especially relevant in regimes where conventional assumptions are no longer adequate. In ultrashort echo time (UTE) imaging of the lung, for example, the signal must be sampled under conditions of extremely rapid T_2^* decay, so that acquisition timing and k-space trajectory become central parts of the signal model itself. In functional methods such as PREFUL, subtle temporal signal variations must be interpreted in relation to physiological processes and motion, linking sequence physics to dynamic tissue behavior. In real-time MRI, finally, the acquisition process is no longer well described as a static encoding problem, but must be understood as a temporally evolving sampling process under strong constraints of speed and reconstruction.

A central motivation of this work is therefore to present MRI in a form in which signal formation, sequence design, and spatial encoding can be understood within a single physical framework. Such a perspective not only clarifies the foundations of conventional imaging, but also provides a natural basis for the analysis and simulation of advanced techniques in which rapid relaxation, motion, undersampling, and non-Cartesian trajectories play a decisive role.

2 Nuclear Spins and the Rotating Frame

2.1 Nuclear Spins and Precession

Atomic nuclei with a non-zero spin possess an intrinsic magnetic moment. In clinical magnetic resonance imaging, the relevant nuclei are primarily hydrogen nuclei (protons), which are abundant in water and fat and therefore widely distributed throughout biological tissue.

The proton carries a quantum mechanical spin, giving rise to a magnetic moment that interacts with external magnetic fields. When placed in a static magnetic field B_0, these magnetic moments preferentially

align either parallel or antiparallel to the field direction.

Due to a slight energy difference between these two states, a small excess of spins occupies the lower-energy (parallel) configuration, resulting in a net magnetization along the direction of the external field.[10, 7]

At thermal equilibrium, a slight excess of spins occupies the lower-energy state aligned parallel to B_0 compared to those aligned antiparallel. This population difference leads to a net macroscopic magnetization vector M_0 oriented along the longitudinal (z-) direction. For an ensemble of spin-$\frac{1}{2}$ nuclei (hydrogen), the equilibrium magnetization is given by

$$M_0 = \frac{N\gamma^2\hbar^2 B_0}{4kT}, \tag{1}$$

where N is the proton density, γ the gyromagnetic ratio, $\hbar$ the reduced Planck constant, k the Boltzmann constant, and T the absolute temperature. Thus, M_0 increases with magnetic field strength and decreases with temperature. In typical MRI, however, temperature effects are small compared with the influence of B_0.

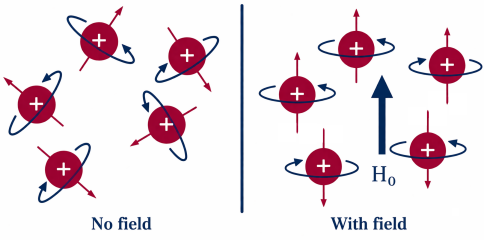

Figure 2.1: Charged particles in magnetic field diagram.

In addition to this alignment, the magnetic moments undergo precessional motion around the direction of the static magnetic field. This motion is described by the Larmor relation

$$\omega_0 = \gamma B_0, \tag{2}$$

where ω_0 is the angular Larmor frequency and γ is the gyromagnetic ratio of the nucleus, with

$$\frac{\gamma}{2\pi} = 42.58\,\text{MHz}\,\text{T}^{-1}.$$

Although the behavior of individual nuclei is governed by quantum mechanics, the observable MR signal arises from an ensemble of a very large number of spins. In this regime, the net magnetization can be described by the expectation value of the spin system, which behaves according to classical equations of motion. [7, 1] This allows the introduction of a macroscopic magnetization vector M.

The precession of the magnetization vector is a fundamental property of magnetic resonance and determines the frequency at which the system can be excited and detected. In equilibrium, the transverse components of the magnetization cancel due to random phase distribution, and no measurable signal is observed.

2.1.1 The Rotating Frame

The precessional motion described by the Larmor relation occurs at radiofrequency frequencies (tens to hundreds of megahertz in clinical MRI). In the laboratory frame, this rapid motion makes it difficult to describe the effect of RF fields and the evolution of the magnetization in an intuitive way.

To simplify the description, it is convenient to introduce a rotating frame of reference that itself rotates about the z-axis at the Larmor frequency ω_0. In this rotating frame, the fast precession of the magnetization around B_0 is effectively removed. As a result, the magnetization appears stationary in equilibrium, rather than undergoing rapid circular motion.

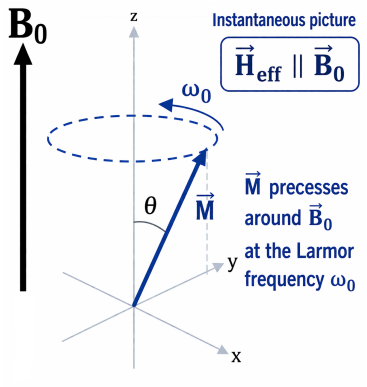

Figure 2.2: MRI vector model and precession diagram.

This transformation has an important consequence: magnetic fields oscillating at the Larmor frequency in the laboratory frame become approximately static fields in the rotating frame. In particular, the RF field $B_1(t)$, which oscillates at frequency ω_0, can be treated as a constant field in the transverse plane. This allows the effect of RF excitation to be described as a simple rotation of the magnetization vector.

In this picture, the dynamics of the magnetization are governed not by the rapid Larmor precession itself, but by deviations from it. Relaxation processes and phase evolution due to gradients or field inhomogeneities therefore appear as comparatively slow changes in the rotating frame.

Throughout the following sections, the behavior of the magnetization will implicitly be described in this rotating frame unless stated otherwise. This provides a more intuitive representation of RF excitation, dephasing, and echo formation in MRI.[7]

In the vector model, the net magnetization is represented as a vector M with longitudinal and transverse components. In equilibrium, only the longitudinal component $M_z = M_0$ is present.

The corresponding Larmor frequencies for typical clinical field strengths are summarized in Table 1.

Table 1: Larmor frequencies for typical clinical field strengths.

Magnetic Field B_0 (T)	Frequency (MHz)
1.5	64
3.0	128
7.0	298

2.2 RF Excitation and Transverse Magnetization

An oscillating magnetic field B_1, applied perpendicular to B_0, rotates the magnetization vector away from the longitudinal direction by a flip angle α. Immediately after excitation, the spins are phase-coherent, resulting in a maximum transverse magnetization M_{xy}.

The transverse magnetization M_{xy}, being perpendicular to B_0, induces a time-varying magnetic flux in a receive coil, giving rise to the measurable MR signal.[10, 7]

In practice, RF excitation and signal detection are realized by dedicated transmit and receive coils, as illustrated in Fig. 2.5.

3 Signal and Echo Formation

3.1 Signal Formation and Dephasing

The MR signal arises from the time-varying transverse magnetization $M_{xy}(t)$ generated by RF excitation, which precesses about the static magnetic field B_0 at the Larmor frequency ω_0. This precession produces

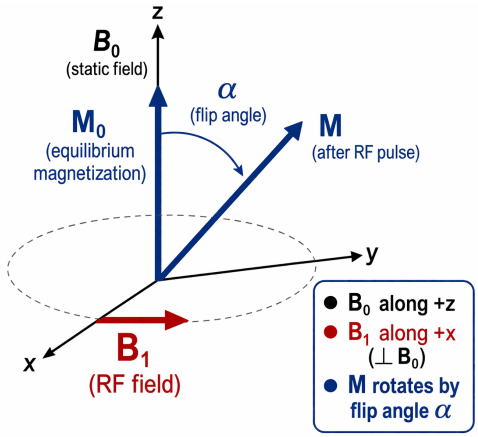

Figure 2.3: Rotation of the magnetization vector M by an RF field B_1, defining the flip angle α.

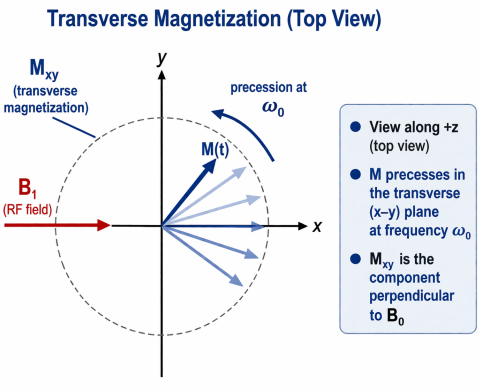

Figure 2.4: Phase coherence in the transverse plane. Immediately after RF excitation, individual spins are aligned in phase, resulting in a maximum transverse magnetization M_{xy}. The magnetization precesses at the Larmor frequency ω_0, forming the basis of the detectable MR signal.

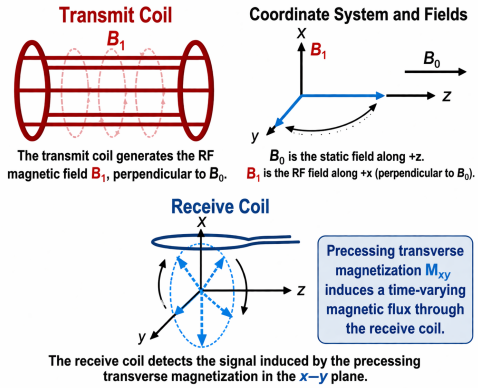

Figure 2.5: Transmit and receive coils in MRI. The RF field B_1, generated by the transmit coil, is perpendicular to B_0 and rotates the magnetization into the transverse plane. The precessing transverse magnetization M_{xy} induces a measurable signal in the receive coil.

a time-varying magnetic flux through the receive coil. According to Faraday's law of induction, the changing flux induces an electromotive force, resulting in a measurable voltage $V(t)$. The detected signal reflects the transverse magnetization and oscillates at the Larmor frequency.

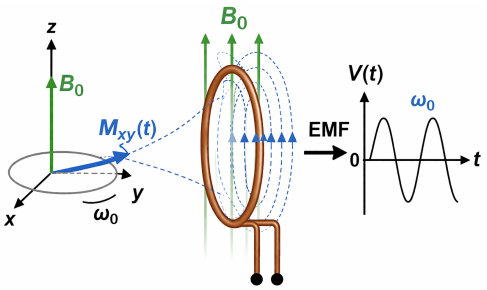

Figure 3.1: Formation and detection of the MR signal. The transverse magnetization $M_{xy}(t)$ precesses at the Larmor frequency ω_0 about the static magnetic field B_0, producing a time-varying magnetic flux in the receive coil. This induces an electromotive force (EMF) and the measured voltage $V(t)$.

After RF excitation, the transverse magnetization $M_{xy}(t)$ is initially phase-coherent, with individual spins precessing in synchrony. Over time, spin-spin interactions and magnetic field inhomogeneities lead to a progressive loss of phase coherence (dephasing), as illustrated in Fig. 3.2. As a result, the net transverse magnetization decreases, even though the magnitude of individual spins remains unchanged. This loss of coherence manifests as a decay of the measured MR signal, observed as the free induction decay (FID), which follows an exponentially damped oscillation characterized by the effective transverse relaxation time T_2^*.

This dephasing can be partially reversed by appropriate RF pulses, forming the basis of spin echo techniques.

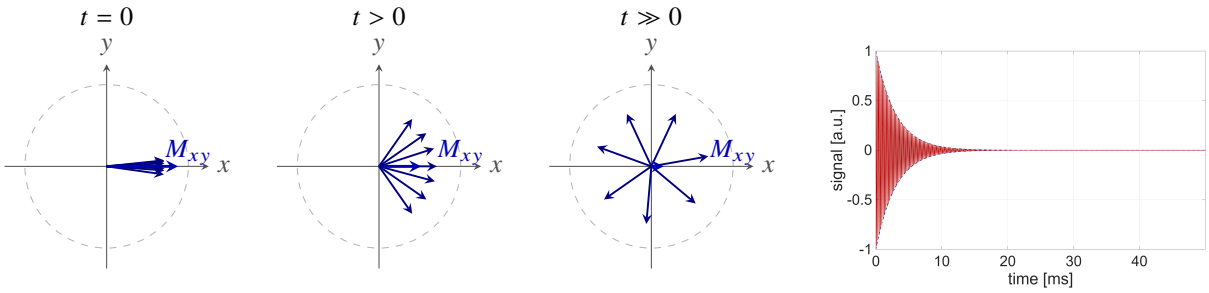

Figure 3.2: Progressive dephasing of transverse magnetization in the transverse plane and the corresponding free induction decay (FID).

3.2 Echo Formation (Spin Echo, Gradient Echo)

The loss of phase coherence following RF excitation can be partially reversed by applying an additional RF pulse. In a spin echo sequence, a 180° pulse is applied after a certain time, inverting the phase distribution of the spins. Spins that were precessing faster now lag behind, while slower spins move ahead.

As a result, the spins re-align in phase at a later time, leading to a temporary recovery of the transverse magnetization. This rephasing produces a measurable signal known as the spin echo.

The spin echo refocuses dephasing caused by magnetic field inhomogeneities, but not the intrinsic loss of coherence due to spin-spin interactions. Therefore, the decay of the spin echo signal is governed by the transverse relaxation time T_2, in contrast to the free induction decay, which is characterized by T_2^*.

In contrast to spin echo sequences, gradient echo techniques do not employ a refocusing RF pulse. Instead, dephasing induced by magnetic field gradients is reversed by switching the gradient polarity.

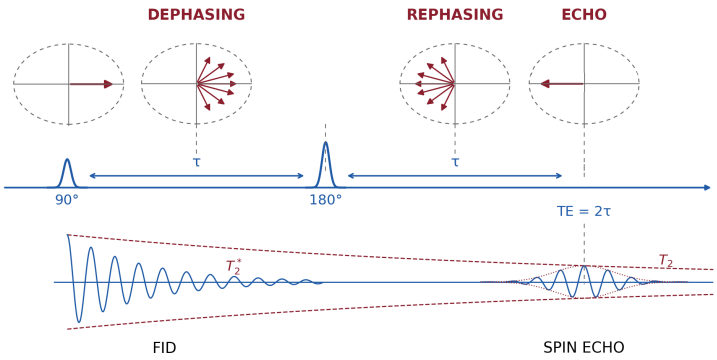

Figure 3.3: Spin echo formation by RF-induced rephasing. After a 90° excitation pulse, spins in the transverse plane progressively lose phase coherence (dephasing), leading to free induction decay (FID). A subsequent 180° pulse inverts the phase distribution of the spins, so that faster and slower spins re-align at time TE = 2τ, producing a spin echo. While the spin echo refocuses dephasing caused by magnetic field inhomogeneities, it does not reverse the intrinsic transverse relaxation described by T_2.

However, this mechanism does not compensate for phase dispersion caused by magnetic field inhomogeneities. Consequently, the signal decay in gradient echo imaging is governed by the effective transverse relaxation time T_2^*.

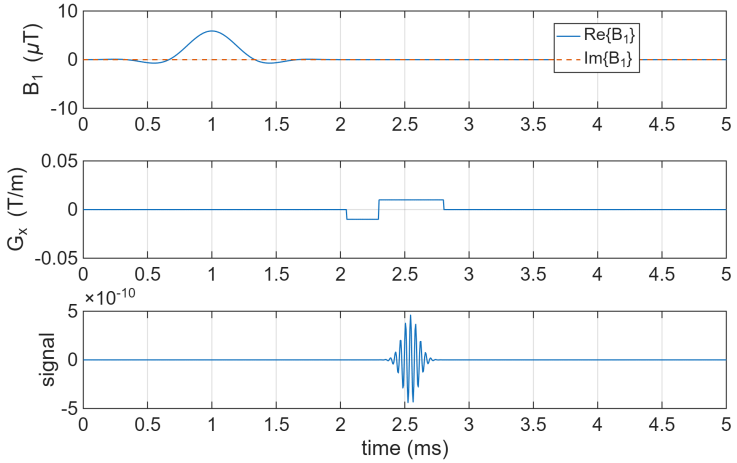

Figure 3.4: Gradient echo signal formation. Following excitation with a flip angle α, a dephasing gradient ($-G$) introduces a controlled phase dispersion across the spins. Reversal of the gradient polarity ($+G$) compensates this gradient-induced dephasing, leading to the formation of a gradient echo at time TE. In contrast to spin echo sequences, no refocusing RF pulse is applied; therefore, phase dispersion caused by magnetic field inhomogeneities is not reversed. Consequently, the signal evolution remains governed by the effective transverse relaxation time T_2^*.

4 Relaxation and Contrast (T_1, T_2, T_2^*)

Following RF excitation, the transverse magnetization $M_{xy}(t)$ is initially phase-coherent, with individual spins precessing in synchrony in the transverse plane. This coherent precession produces a time-varying magnetic flux through the receive coil. According to Faraday's law of induction, the changing flux induces an electromotive force, resulting in a measurable voltage signal $V(t)$ that oscillates at the Larmor frequency ω_0.

Over time, spin-spin interactions and magnetic field inhomogeneities lead to a progressive loss of

phase coherence (dephasing). As a result, the net transverse magnetization decreases, even though the magnitude of individual spins remains unchanged. This loss of coherence manifests as a decay of the measured MR signal, observed as the free induction decay (FID).

The signal decay is characterized by the effective transverse relaxation time T_2^*, which includes both irreversible spin-spin interactions (described by T_2) and reversible dephasing effects due to magnetic field inhomogeneities. While T_2 reflects intrinsic tissue properties, T_2^* is additionally influenced by external field variations and is therefore shorter.

This dephasing can be partially reversed by appropriate RF pulses, forming the basis of spin echo techniques.

Longitudinal and transverse relaxation. Following RF excitation, the magnetization evolves according to two independent relaxation processes. The longitudinal magnetization M_z recovers towards its equilibrium value with a time constant T_1, whereas the transverse magnetization M_{xy} decays due to dephasing with a time constant T_2.

Tissues differ in their relaxation properties. Fat exhibits both a short T_1 and a short T_2, resulting in rapid longitudinal recovery and rapid transverse signal decay. In contrast, water shows longer T_1 and T_2 values, leading to slower recovery and more persistent transverse magnetization. These behaviors are illustrated in Fig. 4.1.

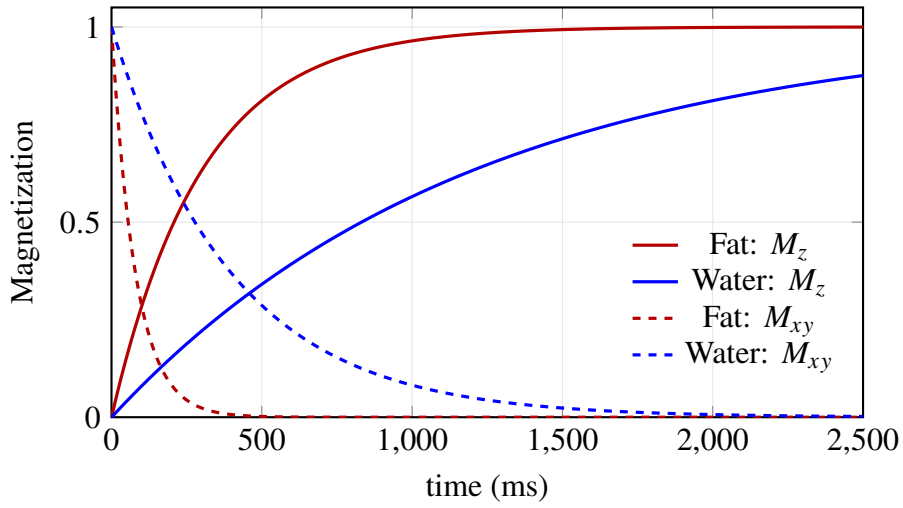

Figure 4.1: Longitudinal (T_1) and transverse (T_2) relaxation for fat and water. Solid lines represent longitudinal recovery (M_z), while dashed lines indicate transverse decay (M_{xy}).

The observed transverse signal decay is influenced by two mechanisms. The intrinsic relaxation time T_2 reflects irreversible spin-spin interactions, whereas the effective relaxation time T_2^* additionally includes dephasing caused by magnetic field inhomogeneities. Consequently, $T_2^* < T_2$, as illustrated in Fig. 4.2.

Image contrast depends not only on tissue properties but also on the acquisition parameters. In a simplified spin-echo model, the signal depends on the repetition time (TR) and echo time (TE) according to

$$S(\mathrm{TR}, \mathrm{TE}) \propto \rho \left(1 - e^{-\mathrm{TR}/T_1}\right) e^{-\mathrm{TE}/T_2}, \tag{3}$$

where ρ denotes the proton density.

Fig. 4.3 shows the dependence of the signal on TR for tissues with different T_1 values, illustrating the origin of T_1 weighting through incomplete longitudinal recovery. Fig. 4.4 displays the signal as a function of TE for different T_2 values, demonstrating how transverse decay leads to T_2 contrast.

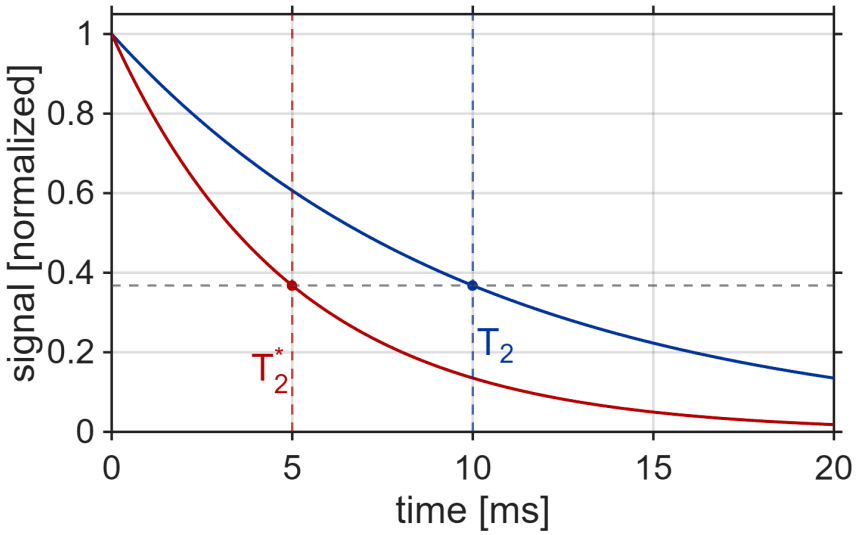

Figure 4.2: Comparison of transverse relaxation times T_2 and T_2^*. Additional dephasing due to magnetic field inhomogeneities leads to a faster signal decay characterized by T_2^*.

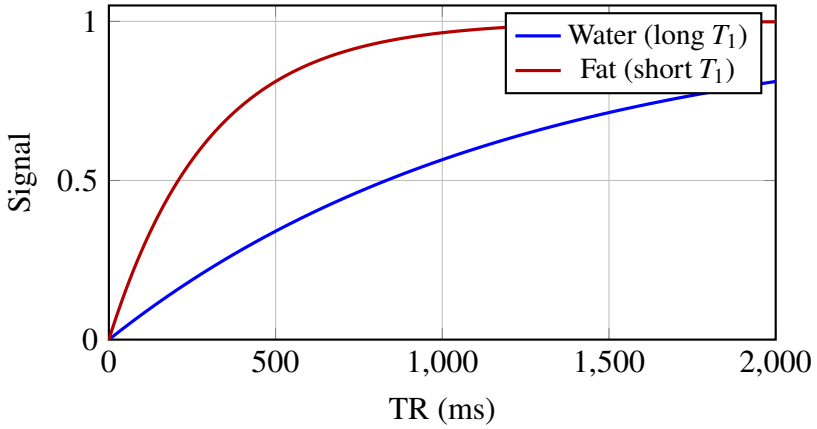

Figure 4.3: Dependence of signal intensity on repetition time (TR) for tissues with different T_1 values. Fat (short T_1) recovers more rapidly than water, leading to higher signal at short TR and thus T_1 weighting.

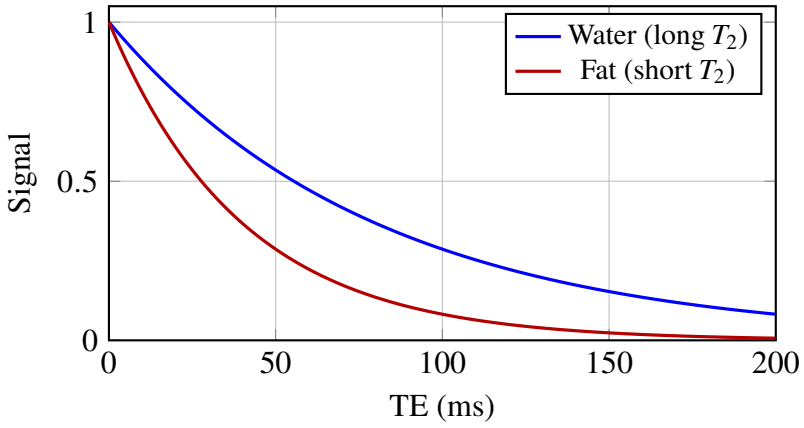

Figure 4.4: Dependence of signal intensity on echo time (TE) for tissues with different T_2 values. Water (long T_2) retains signal longer than fat, leading to T_2 contrast at longer TE.

5 Basic Sequences (SE, GRE)

Having established the physical mechanisms underlying signal formation and rephasing, these concepts can now be extended to complete imaging sequences, in which RF pulses and gradient fields are combined to encode spatial information.

5.1 Spin Echo (SE)

In spin-echo imaging, a 90° RF pulse first rotates the longitudinal magnetization into the transverse plane, where it begins to dephase due to both static field inhomogeneities and intrinsic spin–spin interactions. A subsequent 180° RF pulse reverses the phase dispersion caused by static field variations, leading to a rephasing of the spins and the formation of a spin echo at time TE. In contrast to gradient-echo imaging, this refocusing mechanism compensates for reversible dephasing, so that the echo amplitude is governed predominantly by T_2 relaxation rather than by T_2^* effects.

In multi-spin-echo sequences, a train of 180° pulses generates a series of echoes at successive echo times. The temporal evolution of the RF pulses, gradients, and resulting signal is shown in Fig. 5.1. The echoes exhibit an overall decay due to T_2 relaxation, while small residual variations between neighboring echoes arise from finite pulse durations and remaining coherence pathways.

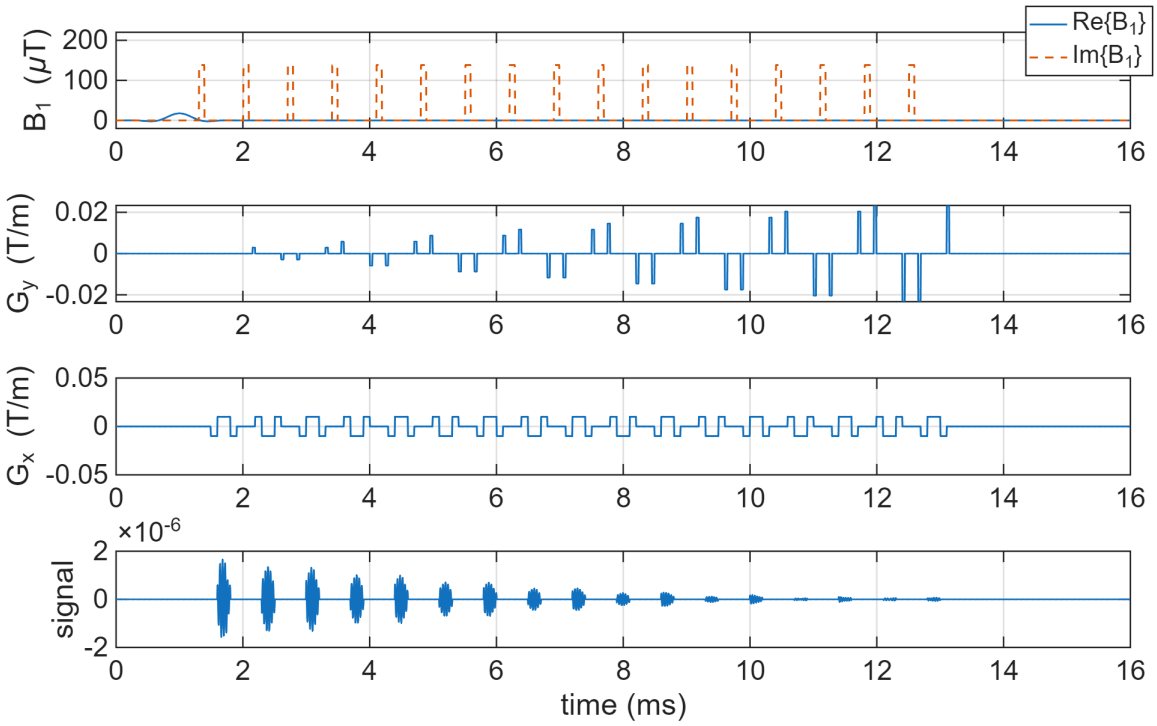

Figure 5.1: Simulated multi-spin-echo sequence. The top panel shows the RF excitation (90°) followed by a train of 180° refocusing pulses. The phase-encoding (G_y) and readout (G_x) gradients generate successive echoes, visible in the bottom panel as a decaying echo train governed predominantly by T_2 relaxation.

The corresponding k-space sampling pattern is illustrated in Fig. 5.3a. Each echo acquires one line of k-space, while the phase-encoding gradient steps through different k_y values. The readout gradient traverses k_x during each echo, resulting in a rectilinear coverage of k-space similar to conventional Cartesian imaging. The symmetry of the sampled region reflects the balanced encoding around the k-space origin.

5.2 Gradient Echo (GRE)

In gradient-echo (GRE) imaging, the signal formation is governed by gradient-induced dephasing and rephasing rather than by RF refocusing. A flip-angle excitation $\alpha < 90°$ is applied during slice selection, after which the transverse magnetization evolves under the influence of magnetic field gradients. The readout gradient first introduces phase dispersion and subsequently reverses it, resulting in a gradient echo at time TE. Because no 180° refocusing pulse is used, static field inhomogeneities are not compensated, and the signal remains sensitive to T_2^* decay.

Figure 5.2 shows a fully simulated multi-echo GRE sequence. The RF excitation, phase-encoding gradient G_y, readout gradient G_x, and the resulting signal evolution are displayed together. The echo train clearly illustrates the progressive T_2^*-induced signal decay across successive echoes, while the oscillatory structure within each echo reflects the continuous phase evolution during readout.

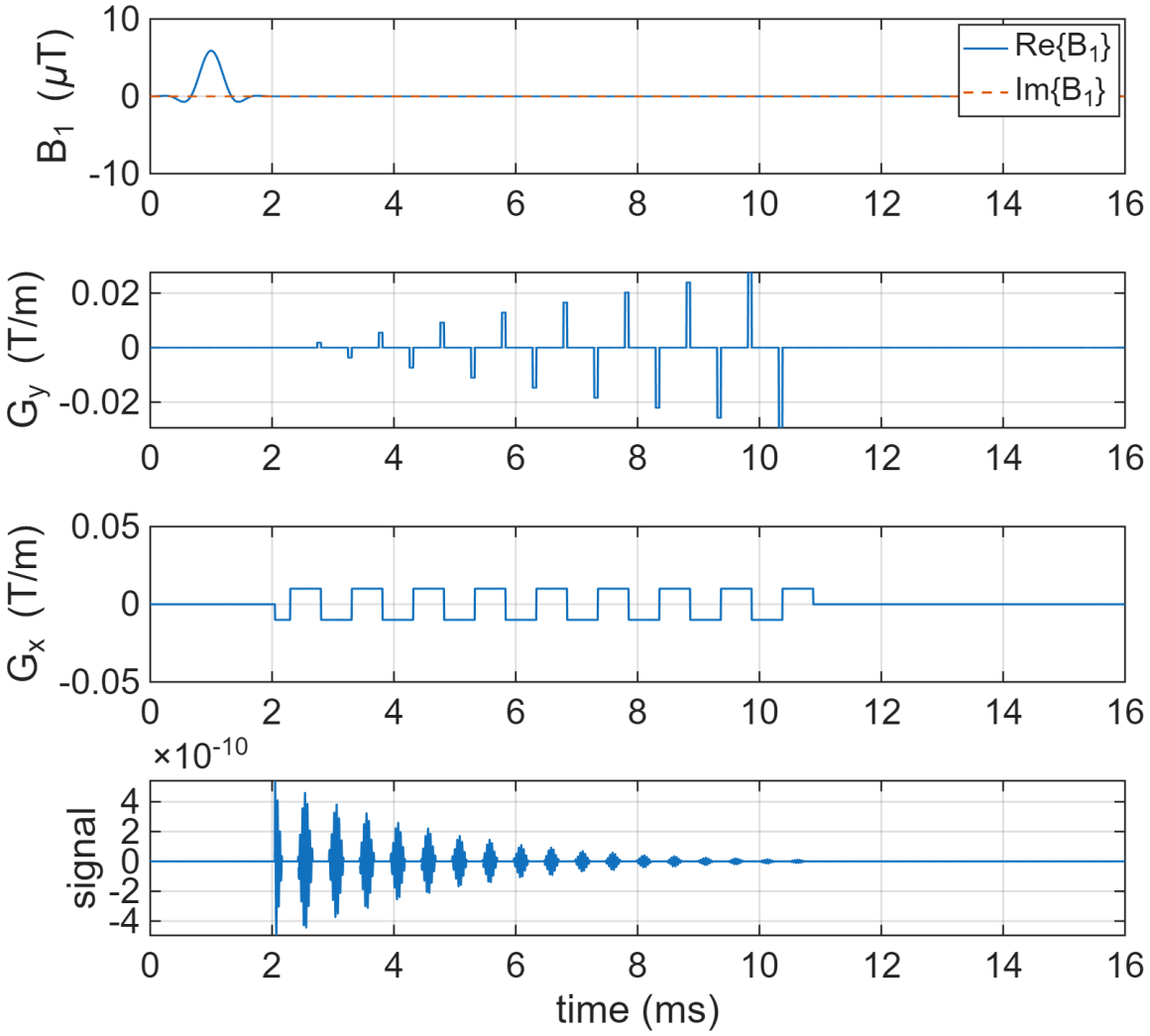

Figure 5.2: Simulated multi-echo gradient-echo sequence. From top to bottom: RF excitation, phase-encoding gradient G_y, readout gradient G_x, and resulting signal. The echo train exhibits T_2^* decay, while each individual echo contains oscillations due to continuous phase accumulation during readout.

The corresponding k-space trajectory is shown in Fig. 5.3b. The readout gradient produces linear traversal along k_x, while the phase-encoding gradient steps the trajectory through discrete k_y positions. The resulting sampling pattern forms a rectilinear grid in k-space, with the ADC active only within a bounded region corresponding to the desired field of view. This illustrates how spatial encoding in GRE imaging is achieved through controlled gradient evolution rather than direct spatial localization.

In steady-state GRE imaging, repeated RF excitations with short repetition times (TR) drive the

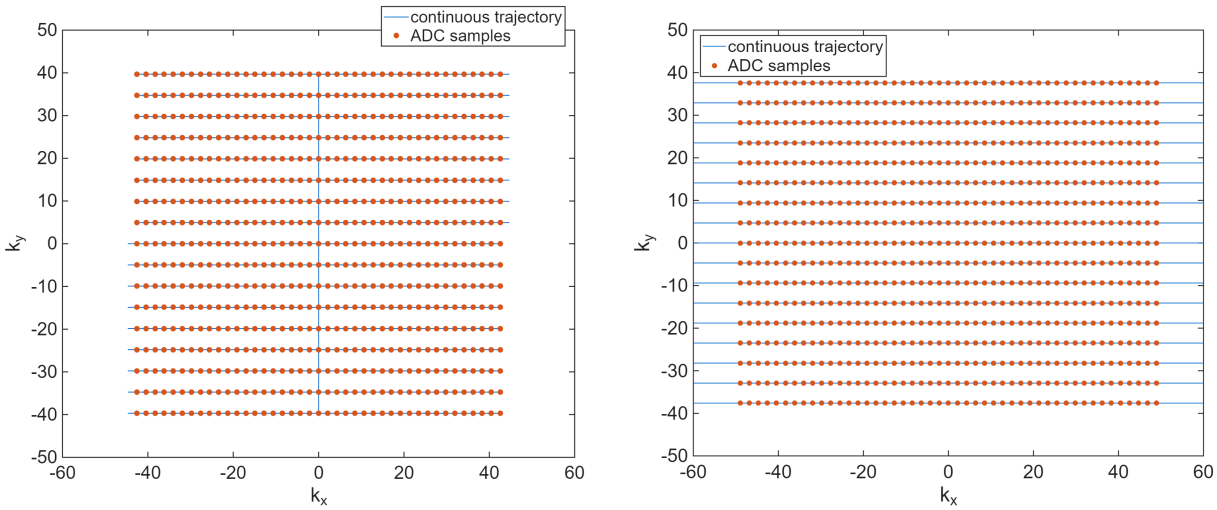

(a) Spin-echo (SE) k-space trajectory.

(b) Gradient-echo (GRE) k-space trajectory.

Figure 5.3: Comparison of Cartesian k-space sampling in multi-echo spin-echo (left) and multi-echo gradient-echo (right) imaging. Continuous lines indicate the gradient-driven trajectory, while orange dots mark ADC sampling points.

magnetization into a partially saturated regime. The signal amplitude is therefore determined by both TR and the flip angle α. For a given TR and longitudinal relaxation time T_1, the signal is maximized at the Ernst angle α_E, defined by $\cos \alpha_E = e^{-\mathrm{TR}/T_1}$. This relationship highlights that saturation effects can be exploited to optimize signal efficiency in rapid imaging sequences rather than merely limiting performance.

5.3 Gradient-Echo vs. Spin-Echo Imaging

Gradient-echo (GRE) and spin-echo (SE) sequences differ fundamentally in how transverse magnetization is generated and refocused, and therefore in how image contrast is formed.

In gradient-echo imaging, transverse magnetization is created by an RF pulse with a flip angle $\alpha < 90°$, and no 180° refocusing pulse is applied. Signal formation relies entirely on gradient-induced dephasing and rephasing. As a consequence, any phase dispersion caused by static field inhomogeneities or susceptibility differences is not corrected. The measured signal therefore decays with an effective time constant T_2^*, which combines irreversible T_2 relaxation with reversible dephasing effects. This makes GRE sequences inherently sensitive to magnetic field variations, which can be exploited for contrast (e.g. susceptibility-weighted imaging or BOLD fMRI), but also leads to signal loss and geometric distortions.

In spin-echo imaging, a 90° RF pulse is followed by one or more 180° refocusing pulses. These pulses reverse the phase dispersion caused by static field inhomogeneities, so that spins rephase and form echoes at well-defined echo times. As a result, the signal decay at the echo maximum is governed predominantly by T_2, with reversible dephasing effectively removed. Spin-echo sequences therefore provide more robust and quantitatively reliable contrast, particularly in regions with strong susceptibility variations.

The two sequence types also differ in their temporal structure and efficiency. Gradient-echo sequences can be implemented with very short repetition times TR and small flip angles, allowing rapid acquisition and efficient coverage of k-space. In contrast, spin-echo sequences require additional RF pulses and longer echo times, which increases energy deposition and limits acquisition speed. Multi-echo spin-echo sequences extend this concept by generating a train of echoes following a single excitation, enabling efficient sampling of multiple k-space lines while maintaining T_2-weighted contrast.

From a practical perspective, GRE sequences are preferred when speed, sensitivity to susceptibility, or steady-state imaging is required, whereas SE sequences are favored when robust T_2 contrast and insensitivity to field inhomogeneities are essential. The choice between the two therefore reflects a

trade-off between physical accuracy of the signal formation and acquisition efficiency.

6 Beyond Basic Sequences

Inversion recovery sequences introduce a preparatory inversion pulse to selectively enhance T_1 contrast by controlling the recovery of longitudinal magnetization.

Fast implementations such as FLASH use low flip angles and short repetition times to enable rapid gradient-echo imaging while maintaining sufficient signal.

6.1 Steady-State Imaging (SSFP)

Steady-state free precession (SSFP) sequences are characterized by the use of short repetition times TR, such that the magnetization does not fully relax between successive RF excitations. As a result, a dynamic equilibrium is established in which both longitudinal and transverse magnetization components persist over many repetitions. The observed signal therefore arises from the continuous evolution of this steady state rather than from a single excitation.

The establishment of this steady state is not instantaneous. Starting from thermal equilibrium, the magnetization first passes through a transient regime before converging toward a dynamic equilibrium. During this approach, the signal may exhibit oscillatory behavior, reflecting the interplay between repeated RF excitation, relaxation, and residual phase evolution. After a sufficient number of repetitions, a stable steady-state signal is reached.

In Fig. 6.1, this convergence is shown by evaluating the signal at the center of each readout. At this time point, gradient-induced phase is refocused, and the signal corresponds to a fixed phase condition in the rotating frame. The plotted quantity therefore represents the magnitude (or phase-aligned component) of the steady-state magnetization and does not exhibit the rapid oscillations that occur during continuous readout. These oscillations, which arise from ongoing phase evolution of the transverse magnetization, are illustrated separately in Fig. 6.2.

A key distinction between different SSFP sequences lies in the treatment of transverse coherence. In unbalanced SSFP sequences (such as FISP or GRASS), residual gradient moments lead to partial dephasing of transverse magnetization between repetitions. Although a steady state is still formed, transverse coherence is only partially preserved, and the signal behavior resembles that of gradient-echo imaging.

In contrast, balanced SSFP (bSSFP) fully compensates all gradient moments within each repetition. This preserves phase coherence of the transverse magnetization across successive RF pulses and establishes a fully coherent steady state. The resulting signal is highly efficient and reflects the combined influence of longitudinal recovery and transverse decay.

Because both T_1 and T_2 processes contribute continuously, the bSSFP signal exhibits a characteristic contrast that is approximately proportional to T_2/T_1. This leads to high signal intensity in tissues with relatively long T_2 and short T_1, such as fluids, and distinguishes bSSFP from conventional spin echo (T_2-weighted) and gradient echo (T_2^*-weighted) imaging.

In balanced SSFP, the RF pulses are typically applied with alternating phase (e.g., $+x$, $-x$, $+x$, ...) in the rotating frame. This phase cycling does not change the flip angle but modifies the phase reference of each excitation. As a result, residual transverse coherences evolve symmetrically over successive repetitions, stabilizing the steady state and reducing sensitivity to off-resonance effects.

Figure 6.2 illustrates a didactic balanced SSFP scheme. A train of low-flip RF pulses with alternating phase is applied at short repetition times, while the gradient waveforms are balanced within each TR such that their net zeroth moments vanish. Under these conditions, transverse coherence is preserved across repetitions, and the measured signal does not arise from isolated refocusing events, as in spin-echo imaging, but from the continuous evolution of a coherent steady state. The plotted signal represents the real-valued receive signal, i.e., a projection of the complex transverse magnetization onto the receiver reference frame, and therefore appears as an oscillatory waveform.

The corresponding k-space sampling pattern is shown in Fig. 6.3. Each repetition samples one horizontal line in k-space during the readout gradient, while the balanced gradients return the trajectory to the center between repetitions. This highlights a characteristic feature of balanced SSFP imaging: although the signal is generated from a coherent steady state, spatial encoding can still be described in the usual k-space framework. The image is therefore reconstructed, as in other Fourier imaging methods, from the acquired samples in spatial-frequency space.

Unlike spin echo or gradient echo sequences, SSFP does not create a new signal in each repetition. Instead, the same magnetization is maintained and dynamically reshaped over time, enabling highly efficient signal generation at very short repetition times.

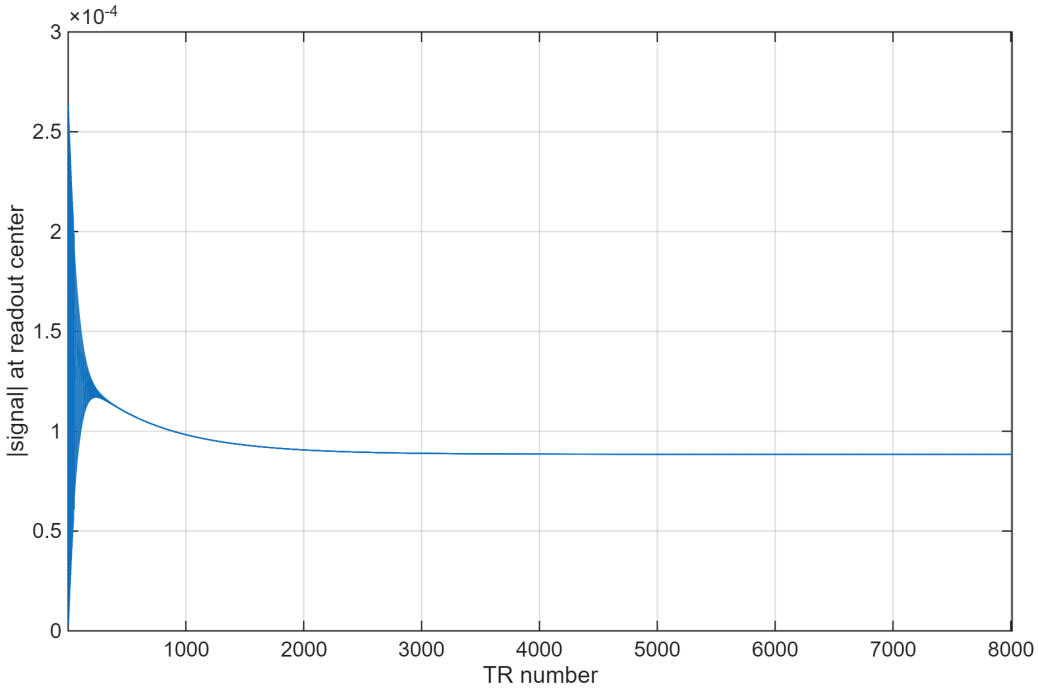

Figure 6.1: Transient approach to steady state in bSSFP. The signal at the center of the readout (the envelope) is shown as a function of repetition number.

The corresponding k-space sampling pattern is shown in Fig. 6.3. Each repetition samples one horizontal line in k-space during the readout gradient, while the balanced gradients return the trajectory to the center between repetitions. This highlights a characteristic feature of balanced SSFP imaging: although the signal is generated from a coherent steady state, spatial encoding can still be described in the usual k-space framework. The image is therefore reconstructed, as in other Fourier imaging methods, from the acquired samples in spatial-frequency space.

Taken together, Figs. 6.2 and 6.3 illustrate the dual character of balanced SSFP imaging: on the one hand, the sequence maintains a coherent steady state of the magnetization over many repetitions; on the other hand, the measured signal is still sampled along well-defined trajectories in k-space and can therefore be reconstructed by Fourier transformation in the usual way.

6.2 Ultra-Fast Imaging: Echo Planar Imaging (EPI)

Ultra-fast imaging techniques aim to acquire large portions of k-space within a single excitation. Two important realizations of this concept are echo planar imaging (EPI) and spiral imaging. In spiral imaging, k-space is traversed along a continuous spiral trajectory, improving acquisition efficiency at the cost of increased sensitivity to field inhomogeneities.

Echo planar imaging (EPI) represents a fundamentally different approach to MR image acquisition, in which a complete image (or a large portion of k-space) is acquired following a single RF excitation.

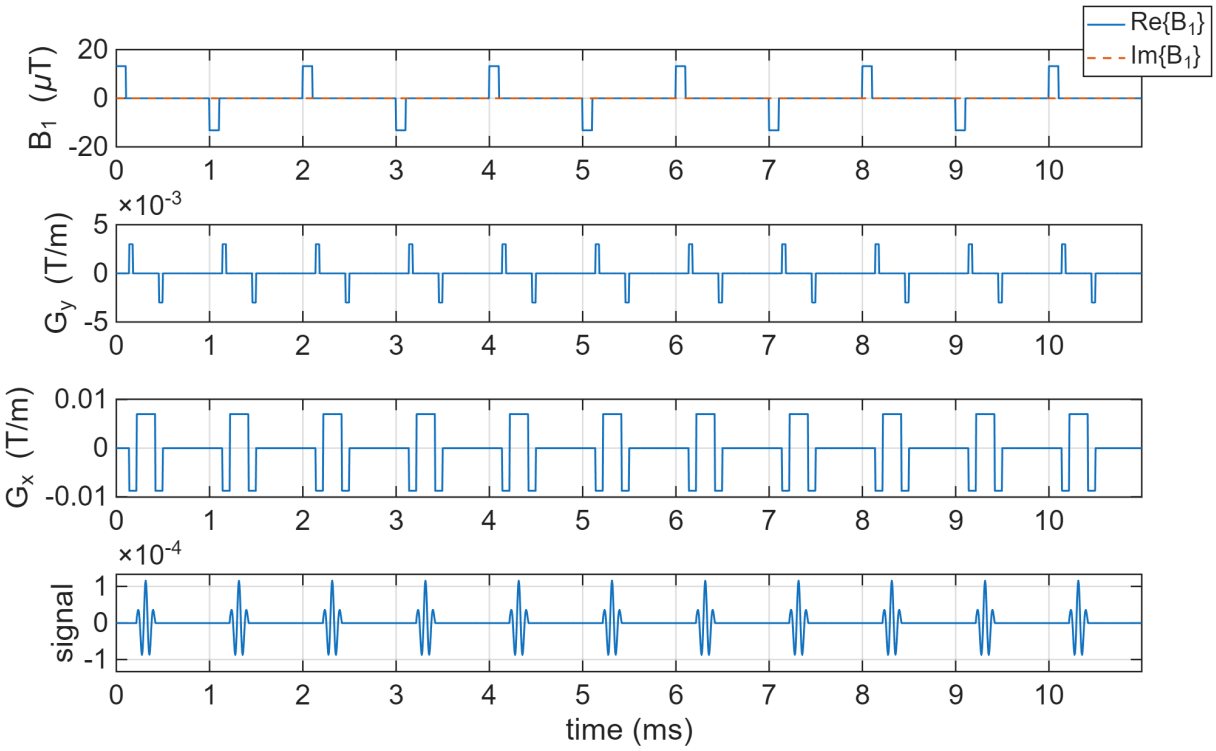

Figure 6.2: Balanced SSFP sequence diagram with alternating RF phase and balanced gradients.

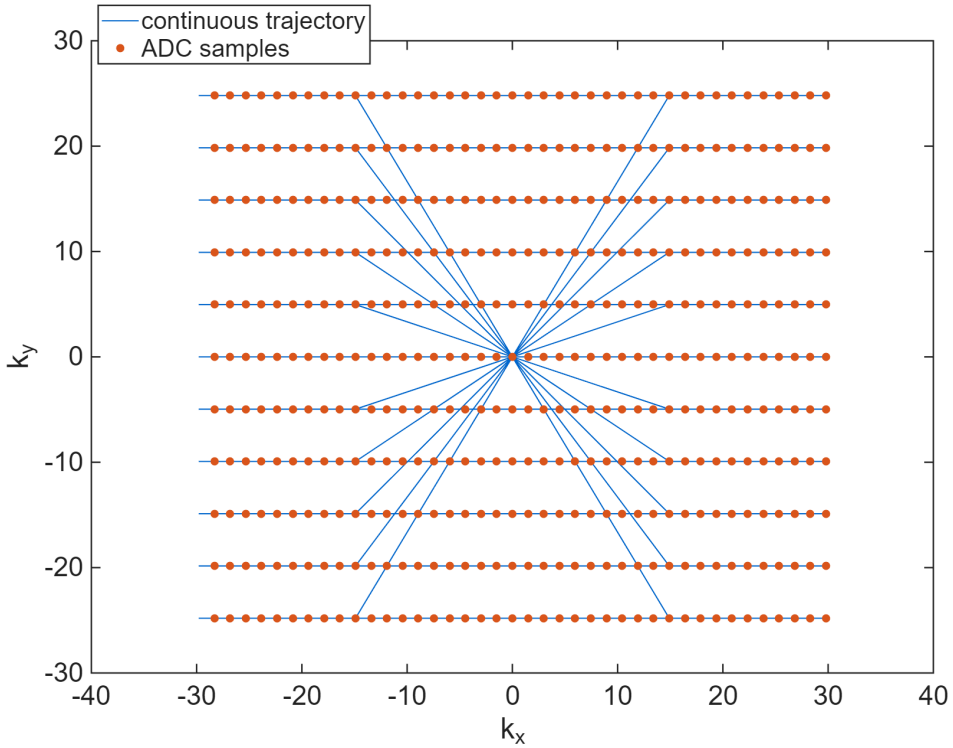

Figure 6.3: Corresponding k-space sampling trajectory in bSSFP.

Table 2: Comparison of transverse magnetization behavior in different MRI sequence types.

	Spin Echo (SE)	**Gradient Echo (GRE)**	**SSFP (balanced)**
Transverse magnetization between repetitions	Refocused by 180° pulse	Dephased (spoiled) after each TR	Preserved across TR
Refocusing mechanism	RF refocusing	Gradient reversal	Gradient balancing
Sensitivity to B_0 inhomogeneity	Reduced	High (T_2^*)	High (banding)
Signal formation	Spin echo	Gradient echo	Steady-state signal
Gradient moments per TR	Not balanced	Not balanced	Fully balanced
Use of spoilers	No	Yes (typical)	No

This is achieved by rapidly traversing k-space using a train of echoes generated by oscillating readout gradients, thereby eliminating the need for repeated excitations for each phase-encoding step.

After a single excitation pulse, a readout gradient is rapidly switched back and forth, while small phase-encoding "blips" increment the position in the k_y direction. As a result, k-space is sampled in a zig-zag (or raster) trajectory, covering multiple lines within one repetition.

In contrast to conventional spin echo or gradient echo imaging, where each repetition samples only a single line in k-space, EPI acquires many (or all) lines within a single shot. This leads to extremely short acquisition times, enabling applications such as diffusion imaging and functional MRI (fMRI).

However, the long readout train makes EPI highly sensitive to T_2^* decay and magnetic field inhomogeneities. As a result, signal loss, geometric distortions, and susceptibility artifacts are more pronounced than in conventional sequences.

EPI can be implemented in different forms. In spin-echo EPI (SE-EPI), a 180° refocusing pulse is inserted to restore phase coherence and reduce sensitivity to magnetic field inhomogeneities, resulting in signal evolution governed predominantly by T_2 decay. In gradient-echo EPI (GE-EPI), no refocusing pulse is applied, and the signal therefore follows T_2^* decay, making it more sensitive to susceptibility effects.

In gradient-echo EPI, excitation is typically performed with a flip angle $\alpha < 90°$, commonly in the range 10°–60°, depending on sequence design and repetition time.

The corresponding k-space trajectories are shown in Fig. 6.6. In both implementations, the oscillating readout gradient produces a rapid traversal along k_x, while the phase-encoding blips increment the position in the k_y direction between successive echoes, resulting in a characteristic zig-zag sampling pattern.

In spin-echo EPI (left), the central region of k-space is sampled near the refocusing time, so that the dominant signal contribution reflects T_2 weighting. In contrast, gradient-echo EPI (right) samples k-space under continuous T_2^* decay, so that both the center and outer regions are affected by susceptibility-induced dephasing. This difference directly links the signal evolution shown above to the resulting k-space weighting.

Spiral imaging. An alternative ultra-fast acquisition strategy is spiral imaging, in which k-space is traversed along a continuous spiral trajectory rather than line-by-line. This is achieved by simultaneously varying the two in-plane gradients, so that the readout follows a rotating trajectory through k-space after a single excitation.

In its most common implementation, spiral imaging is performed as a gradient-echo sequence with flip angle α. The resulting signal is therefore sensitive to T_2^* decay and magnetic field inhomogeneities. Because the trajectory repeatedly passes through the center of k-space, spiral imaging can achieve high acquisition efficiency and improved motion robustness compared with Cartesian echo planar imaging.

However, spiral imaging requires more complex reconstruction, since the acquired data do not lie on

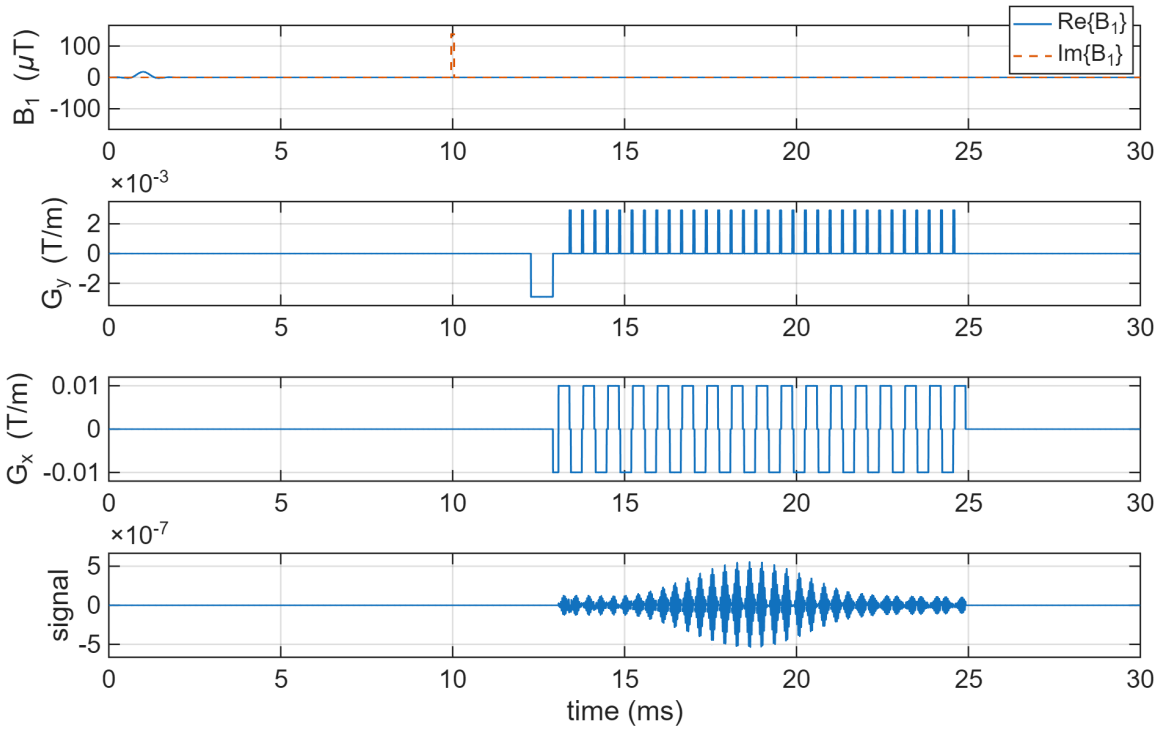

Figure 6.4: Spin-echo EPI (SE-EPI). A 180° refocusing pulse restores phase coherence, leading to a spin-echo maximum at TE. The echo train is modulated by T_2 decay rather than T_2^*, reducing sensitivity to field inhomogeneities.

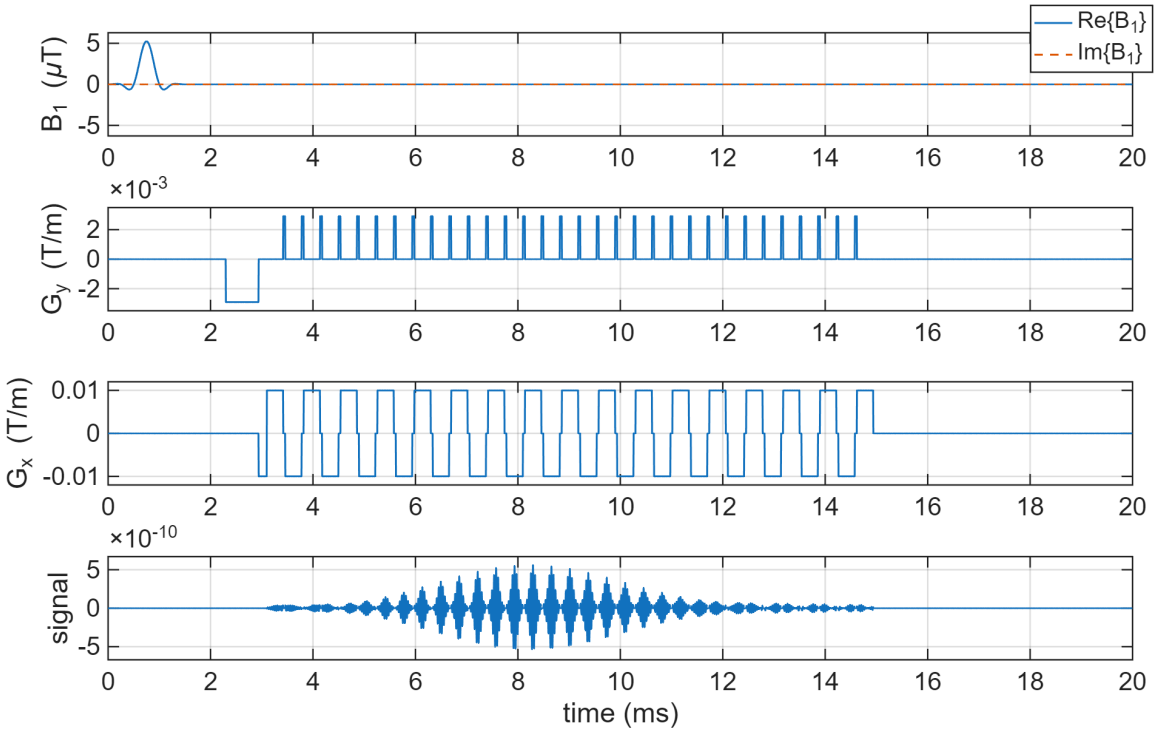

Figure 6.5: Gradient-echo EPI (GE-EPI). Following a single excitation, an oscillating readout gradient generates a train of gradient echoes while phase-encoding blips step through k_y. The signal decays continuously according to T_2^*.

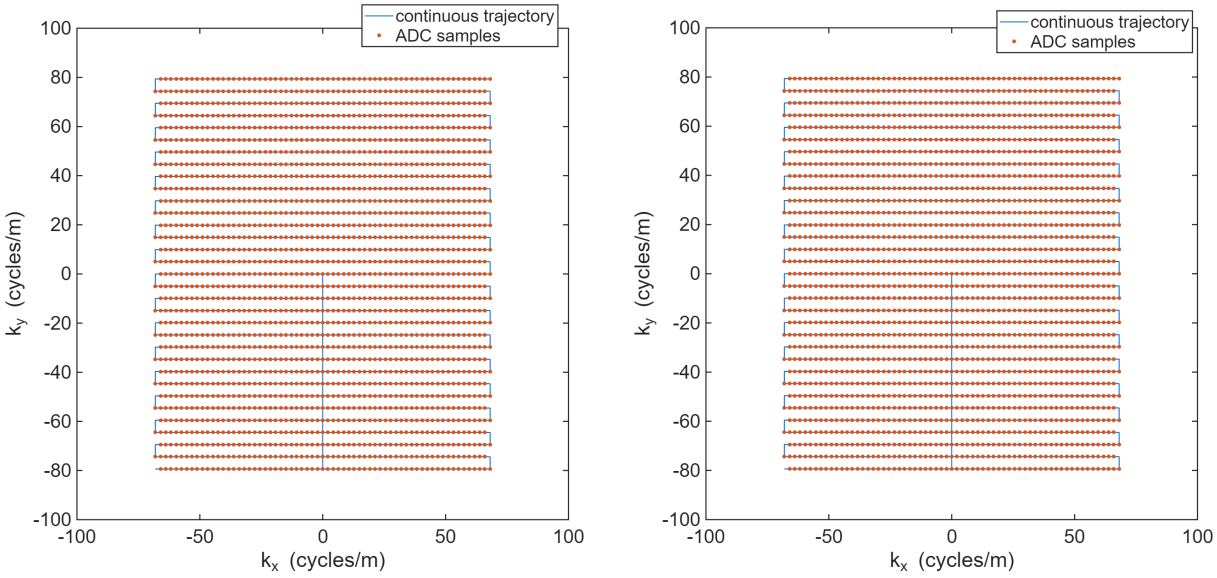

(a) Spin-echo EPI k-space trajectory.

(b) Gradient-echo EPI k-space trajectory.

Figure 6.6: Comparison of k-space sampling in echo planar imaging (EPI). Left: spin-echo EPI with refocused phase evolution. Right: gradient-echo EPI with continuous T_2^*-weighted signal decay. Continuous lines indicate the gradient-driven trajectory, and dots represent ADC samples.

a Cartesian grid and must be interpolated prior to Fourier transformation. Spiral imaging can also be combined with a spin-echo refocusing pulse to reduce sensitivity to field inhomogeneities, although this is less commonly used than gradient-echo spiral imaging.

The corresponding spiral sequence diagrams are shown in Figs. 6.7 and 6.8, while the associated k-space trajectories are compared in Fig. 6.9.

7 Spatial Encoding

7.1 Spatial Encoding (Conceptual)

All encoding mechanisms introduced so far can be understood as specific realizations of a more general principle: the controlled accumulation of position-dependent phase in the transverse magnetization. This perspective leads naturally to the concept of k-space.

In this framework, the acquired MR signal does not directly represent spatial position, but rather a superposition of spatial frequency components.

The measured data are described in so-called *k-space*. The center of k-space contains low spatial frequencies, which determine the overall signal intensity and contrast of the image, whereas the outer regions contain high spatial frequencies, which encode fine spatial details and edges. The acquisition process can therefore be interpreted as sampling different spatial frequency components of the object.

7.1.1 Classical encoding view

In the conventional description, spatial encoding is achieved through slice selection, phase encoding, and frequency encoding gradients. Slice selection restricts the signal to a defined spatial region, while phase and frequency encoding introduce position-dependent phase and frequency shifts within the slice. By varying these gradients across repetitions and during readout, spatial information can be resolved in all three dimensions. In the more general framework, these operations correspond to sampling the spatial frequency domain (k-space).

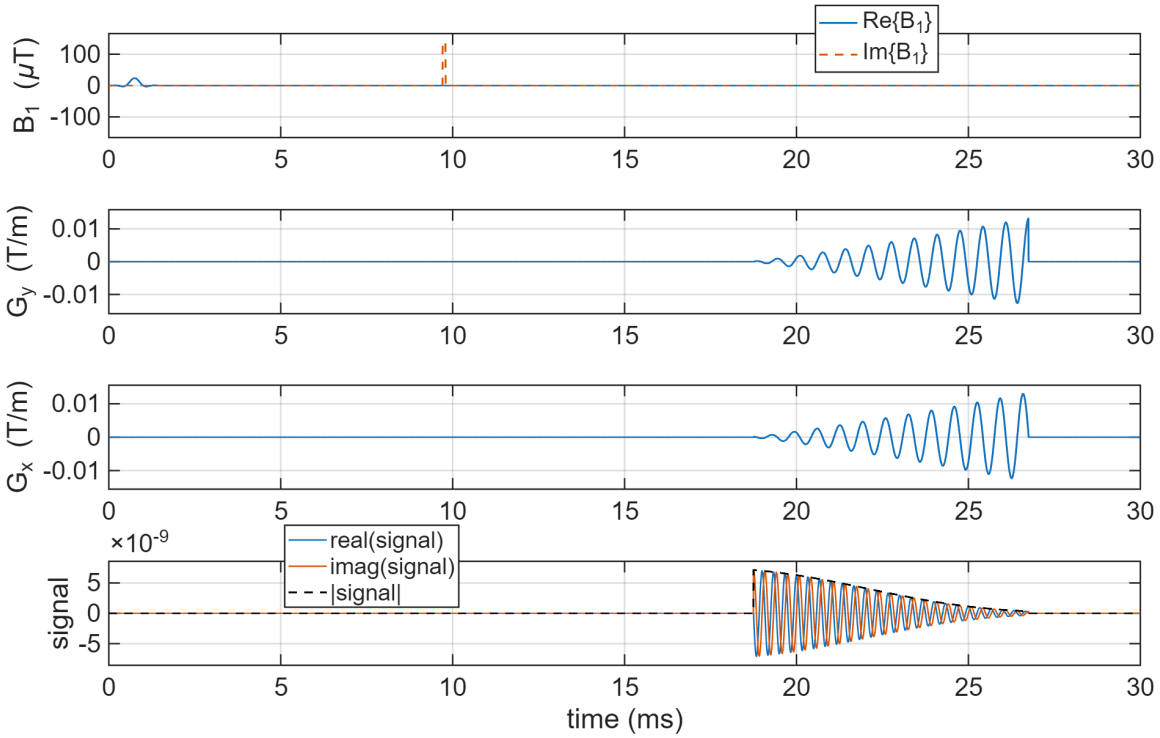

Figure 6.7: Spin-echo spiral imaging. A 180° refocusing pulse restores phase coherence, while a continuous spiral readout samples k-space. The signal evolution is governed predominantly by T_2 decay, reducing sensitivity to field inhomogeneities compared to gradient-echo spiral imaging.

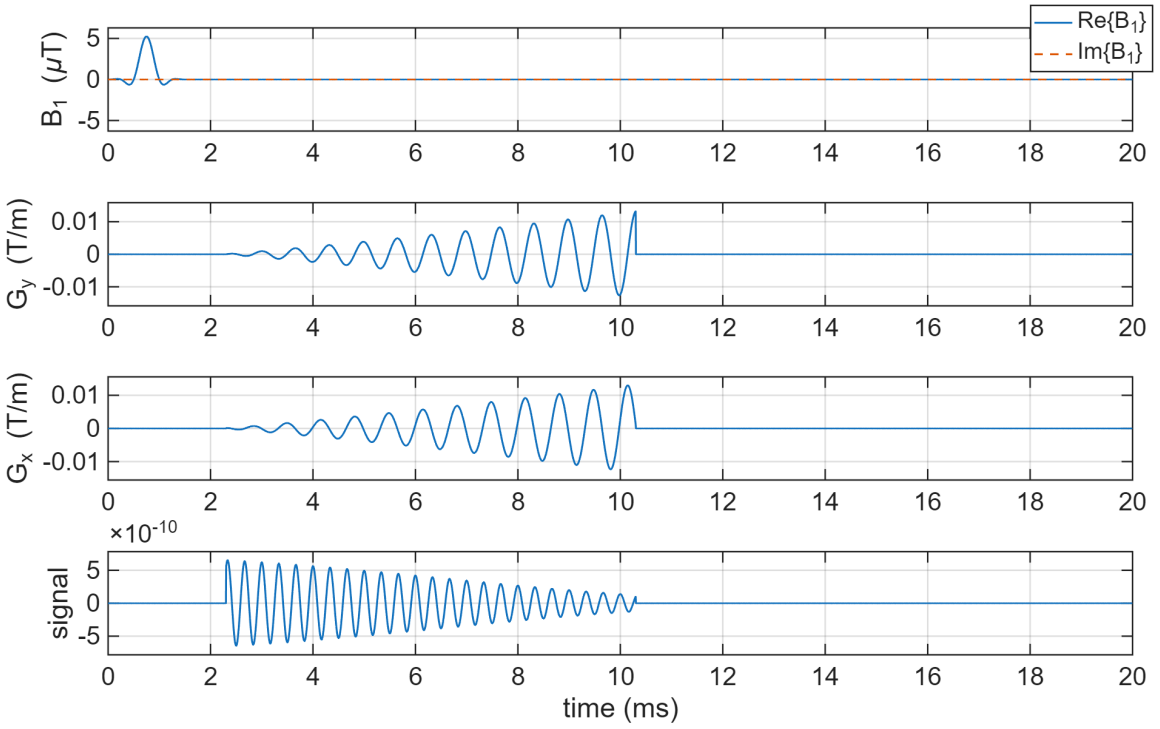

Figure 6.8: Gradient-echo spiral imaging. After excitation with flip angle α, a continuous spiral readout samples k-space from the center outward. The signal is acquired continuously and decays according to T_2^*, making it sensitive to field inhomogeneities.

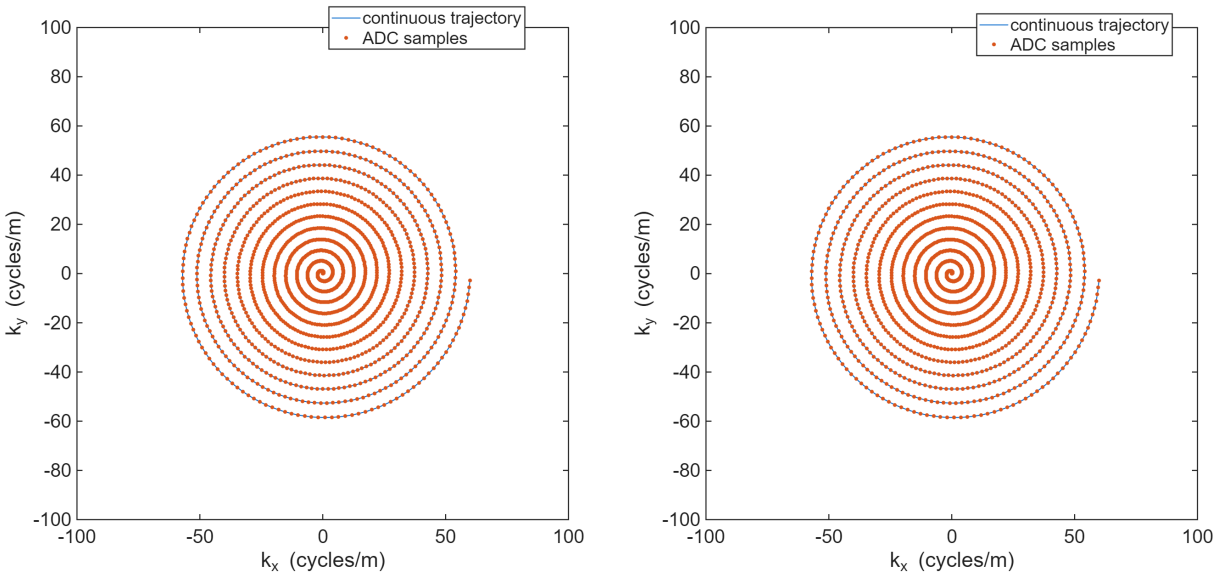

(a) Spin-echo spiral k-space trajectory.

(b) Gradient-echo spiral k-space trajectory.

Figure 6.9: Comparison of spiral k-space sampling. Left: spin-echo spiral with refocused phase at the center. Right: gradient-echo spiral with continuous outward traversal and T_2^*-weighted signal decay.

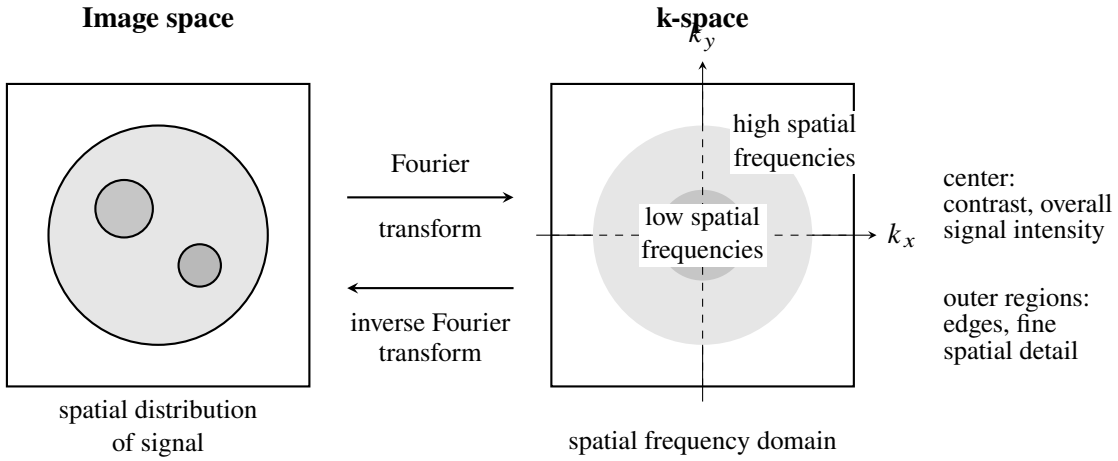

Figure 7.1: Conceptual relation between image space and k-space. The image is represented in real space by the spatial distribution of signal intensity, whereas the measured MR data are acquired in k-space, the spatial frequency domain. The center of k-space contains low spatial frequencies and primarily determines overall image contrast and signal intensity, while the outer regions contain high spatial frequencies and encode fine structural detail and edges. The image is reconstructed from k-space by inverse Fourier transformation.

7.2 Spatial Encoding (Mathematical Formulation)

The spatial encoding of the MR signal can be described quantitatively by considering the phase evolution of the transverse magnetization in the presence of magnetic field gradients.

In the presence of a gradient field $\mathbf{G}(t) = (G_x(t), G_y(t), G_z(t))$, the Larmor frequency becomes position-dependent:

$$\omega(\mathbf{r}, t) = \gamma \left(B_0 + \mathbf{G}(t) \cdot \mathbf{r}\right),$$

where γ is the gyromagnetic ratio and $\mathbf{r} = (x, y, z)$ denotes spatial position.

The accumulated phase at time t is therefore given by

$$\phi(\mathbf{r}, t) = \int_0^t \omega(\mathbf{r}, \tau)\, d\tau = \gamma \int_0^t \mathbf{G}(\tau)\, d\tau \cdot \mathbf{r} + \gamma B_0 t.$$

The constant term $\gamma B_0 t$ does not contribute to spatial encoding after demodulation and can therefore be omitted. Defining the *k-space trajectory* as

$$\mathbf{k}(t) = \frac{\gamma}{2\pi} \int_0^t \mathbf{G}(\tau)\, d\tau,$$

the phase can be written as

$$\phi(\mathbf{r}, t) = 2\pi\, \mathbf{k}(t) \cdot \mathbf{r}.$$

The measured MR signal corresponds to the superposition of all transverse magnetization contributions:

$$s(t) = \int \rho(\mathbf{r})\, e^{i\phi(\mathbf{r},t)}\, d\mathbf{r} = \int \rho(\mathbf{r})\, e^{i2\pi \mathbf{k}(t)\cdot\mathbf{r}}\, d\mathbf{r},$$

where $\rho(\mathbf{r})$ denotes the spin density.

This expression shows that the measured signal $s(t)$ represents samples of the Fourier transform of the object $\rho(\mathbf{r})$ at positions $\mathbf{k}(t)$ in k-space. The image is therefore obtained by inverse Fourier transformation:

$$\rho(\mathbf{r}) = \int s(\mathbf{k})\, e^{-i2\pi \mathbf{k}\cdot\mathbf{r}}\, d\mathbf{k}.$$

Thus, the applied gradient waveforms $\mathbf{G}(t)$ define a trajectory $\mathbf{k}(t)$ in k-space, and the pulse sequence determines how this spatial frequency space is sampled.

8 Lung MRI: Acquisition and Functional Imaging

Magnetic resonance imaging of the lung presents a distinct set of challenges compared to most other organs. The combination of low proton density and strong susceptibility differences at air–tissue interfaces leads to rapid signal decay, often on the order of very short T_2^* times. In addition, the lung is subject to continuous and comparatively fast motion due to respiration and cardiac activity, which can cause substantial image degradation.

As a consequence, lung MRI operates in a regime in which both signal formation and signal encoding are severely constrained. Conventional Cartesian imaging strategies are often unable to capture sufficient signal before decay occurs, while motion further complicates spatial encoding and image reconstruction [9, 6].

For this reason, lung MRI requires both adapted acquisition strategies and specialized approaches for extracting meaningful physiological information from the measured signal.

A useful conceptual distinction can be made between two levels of description in MRI. On the one hand, acquisition strategies determine how the MR signal is sampled under physical constraints such as rapid relaxation and motion. On the other hand, functional methods aim at extracting physiological information from the acquired data, for example by analyzing temporal signal variations. These two

levels address different aspects of the imaging process and are, to a large extent, independent of each other.

In practice, however, both levels must work together: acquisition defines what signal is available, while functional analysis determines how this signal is interpreted. This interplay is particularly important in lung MRI, where both signal formation and physiological dynamics are strongly constrained.

From a broader perspective, recent developments in lung MRI increasingly combine non-Cartesian ultrashort-echo-time (UTE) acquisition with model-based or data-driven analysis frameworks. Acquisition techniques aim to preserve signal under adverse physical conditions, whereas functional methods exploit temporal dynamics to infer ventilation and perfusion [3, 8, 12].

The following examples illustrate this general principle:

- Acquisition strategies (e.g., FLORET) address how the MR signal is sampled under physical constraints.
- Functional methods (e.g., PREFUL) address how physiological information is extracted from the acquired data.

These two levels are conceptually distinct but can be combined within a single imaging framework. This can be illustrated by contrasting an acquisition strategy (FLORET) with a functional analysis method (PREFUL), which together demonstrate how lung MRI integrates sequence design with physiological modeling to enable both structural and functional characterization without the use of ionizing radiation or contrast agents.

8.1 Acquisition Strategies: Example of FLORET

Lung MRI is fundamentally constrained by low proton density and extremely short T_2^* relaxation times, which lead to rapid signal decay and reduced signal-to-noise ratio. As a consequence, conventional Cartesian imaging approaches are often insufficient, as they fail to sample the signal before substantial decay occurs [9, 6].

From the general signal model

$$s(t) = \int \rho(\mathbf{r})\, e^{i2\pi \mathbf{k}(t)\cdot \mathbf{r}}\, d\mathbf{r},$$

it follows that the choice of the k-space trajectory $\mathbf{k}(t)$ directly determines how efficiently the available signal is sampled in time.

To address these limitations, ultrashort echo time (UTE) acquisition strategies employ center-out trajectories that begin sampling at $k \approx 0$ immediately after excitation, thereby capturing signal before significant T_2^* decay occurs. A representative example is the *Fermat Loop Ordered Encoding Trajectory* (FLORET), which combines features of radial and spiral sampling within a three-dimensional framework [11].

In FLORET, the trajectory can be interpreted as a set of smoothly varying interleaves that follow quasi-spiral paths on a sphere in k-space. The sampling locations are distributed according to a Fermat spiral, leading to an approximately uniform angular coverage. In simplified form, such trajectories can be written as

$$\mathbf{k}(t) = k_{\max}(t)\, \mathbf{u}(\theta(t), \phi(t)),$$

where $\mathbf{u}$ denotes a direction on the unit sphere and the angular parameters (θ, ϕ) follow a quasi-uniform distribution.

This construction ensures that low spatial frequencies are sampled early, while higher spatial frequencies are acquired later during the readout. Since the signal evolves as

$$s(t) \propto e^{-t/T_2^*},$$

this ordering improves the effective signal-to-noise ratio by assigning the strongest signal contributions to the center of k-space, which dominates image contrast.

From a conceptual perspective, FLORET operates at the level of signal acquisition. Its primary objective is to optimize the trajectory $\mathbf{k}(t)$ such that the available transverse magnetization is sampled as efficiently as possible under conditions of rapid decay and motion. As such, it provides a flexible foundation that can be combined with different contrast mechanisms and reconstruction strategies in lung MRI.

8.2 Functional Imaging Without Contrast: Example of PREFUL

Beyond structural imaging, lung MRI increasingly aims at functional characterization of ventilation and perfusion. In this context, *Phase-Resolved Functional Lung MRI* (PREFUL) provides a method to extract functional information without the use of exogenous contrast agents [2, 5].

In contrast to acquisition strategies, PREFUL operates at the level of signal interpretation. The starting point is a time-resolved MR signal

$$s(\mathbf{r}, t),$$

which is acquired during free breathing using fast gradient-echo or UTE-based sequences.

At each spatial location, the measured signal can be modeled as a superposition of physiological components:

$$s(\mathbf{r}, t) = s_0(\mathbf{r}) + \Delta s_{\text{resp}}(\mathbf{r}, t) + \Delta s_{\text{card}}(\mathbf{r}, t),$$

where Δs_{resp} reflects respiratory motion (ventilation) and Δs_{card} reflects cardiac pulsation (perfusion).

These components exhibit characteristic temporal behavior. In a simplified representation, they can be approximated as quasi-periodic modulations:

$$\Delta s_{\text{resp}}(t) \sim A_{\text{resp}} \cos(\omega_{\text{resp}} t + \phi_{\text{resp}}), \qquad \Delta s_{\text{card}}(t) \sim A_{\text{card}} \cos(\omega_{\text{card}} t + \phi_{\text{card}}),$$

with distinct frequency ranges for respiration and cardiac activity.

PREFUL exploits this separation by performing a phase-resolved analysis of the temporal signal evolution. By sorting the signal according to respiratory and cardiac phase, spatial maps of ventilation and perfusion can be reconstructed without external contrast agents [2, 8].

From a conceptual perspective, PREFUL does not define a specific acquisition scheme, but rather a model for decomposing the measured signal into physiologically meaningful components. It therefore complements acquisition strategies such as FLORET: while the latter determines how the signal is sampled in k-space, PREFUL determines how the resulting time-resolved signal is interpreted.

This combination enables functional lung imaging under conditions of rapid signal decay and continuous motion, particularly when PREFUL is applied to data acquired with UTE or FLORET-based trajectories [4].

Summary of Approaches

Table 3: Conceptual comparison of acquisition and functional approaches in lung MRI.

Method	**Level**	**Strength**	**Limitation**
UTE / FLORET	Acquisition	Captures signal at very short T_2^*; robust to motion	Low SNR; non-Cartesian reconstruction complexity
PREFUL	Functional	No contrast agent; simultaneous ventilation and perfusion mapping	Model-based; sensitive to temporal stability
EPI (classical)	Acquisition	Very fast acquisition	Strong distortions; T_2^* sensitivity

From the perspective developed in this work, lung MRI highlights a central aspect of MRI more generally: the measured signal must be understood as the result of a dynamic sampling process in k-space, while its interpretation depends on the temporal and physiological context. Acquisition and analysis therefore represent complementary components of a single signal model, rather than independent processing steps.

9 Conclusion and Outlook

Magnetic resonance imaging can be understood as a process of controlled signal generation, in which nuclear spin dynamics, electromagnetic fields, and acquisition strategies interact to produce measurable data. Although the fundamental physical principles are well established, many contemporary applications operate in regimes in which these principles must be considered in a more integrated and dynamic framework.

Starting from the behavior of spins in a magnetic field, the mechanisms of excitation, relaxation, dephasing, and echo formation lead naturally to the development of pulse sequences and spatial encoding strategies. From this perspective, different sequence types are not merely technical variants, but specific ways of shaping the evolution of magnetization and of determining how the resulting signal is sampled.

This becomes particularly important in advanced applications such as lung imaging with ultrashort echo times, functional MRI methods based on dynamic signal changes, and real-time acquisition techniques with severe temporal constraints. In such settings, the distinction between signal formation, encoding, and reconstruction becomes less clear-cut, and the trajectory through k-space must itself be regarded as part of the physical model.

The framework developed in this document emphasizes the interpretation of MRI as a dynamical sampling process in k-space, governed by the interplay of spin evolution and gradient control. This viewpoint provides a unified basis for understanding both conventional and more advanced imaging methods, including rapid gradient-echo techniques, steady-state imaging, echo planar imaging, and non-Cartesian acquisition strategies.

Future work may extend this approach toward quantitative and functional imaging under more realistic conditions, including motion, field inhomogeneities, and accelerated or undersampled acquisition. In this way, a physically grounded and simulation-oriented treatment of MRI can contribute not only to conceptual understanding, but also to the development and evaluation of clinically relevant imaging methods.

References

[1] Mara Cercignani, Nicholas G. Dowell, and Paul S. Tofts, editors. *Quantitative MRI of the Brain: Principles of Physical Measurement*. CRC Press, 2 edition, 2017.

[2] Martha Dohna, Andreas Voskrebenzev, Filip Klimeš, Till F. Kaireit, Julian Glandorf, Sophia T. Pallenberg, Felix C. Ringshausen, Gesine Hansen, Diane Miriam Renz, Frank Wacker, Anna-Maria Dittrich, and Jens Vogel-Claussen. PREFUL MRI for monitoring perfusion and ventilation changes after elexacaftor-tezacaftor-ivacaftor therapy for cystic fibrosis: A feasibility study. *Radiology: Cardiothoracic Imaging*, 6(2):e230104, 2024.

[3] Chuan T. Foo, David Langton, Bruce R. Thompson, and Francis Thien. Functional lung imaging using novel and emerging MRI techniques. *Frontiers in Medicine*, 10:1125322, 2023.

[4] Filip Klimeš et al. Quantifying spatial and dynamic lung abnormalities with 3d PREFUL FLORET UTE. *Magnetic Resonance in Medicine*, 2025. Metadata to be completed from final published version.

[5] Filip Klimeš, Chuan T. Foo, Marcel Gutberlet, Andreas Voskrebenzev, Richard McIntyre, Marius M. Wernz, Norman Kornemann, Rimma Kondrashova, Robin A. Müller, Robert Grimm, Frank Wacker, Francis Thien, and Jens Vogel-Claussen. Dual-center repeatability, consistency, and comparison of 3d phase-resolved functional (PREFUL) ventilation MRI at 3 and 1.5T in healthy volunteers. *NMR in Biomedicine*, 38:e70101, 2025.

[6] Peder E. Z. Larson. Lung imaging with UTE MRI, 2024. Review manuscript / educational chapter PDF supplied by user.

[7] Donald W. McRobbie, Elizabeth A. Moore, Martin J. Graves, and Martin R. Prince. *MRI: From Picture to Proton*. Cambridge University Press, 2 edition, 2006.

[8] Simon M. F. Triphan, Grzegorz Bauman, Philip Konietzke, Marilisa Konietzke, and Mark O. Wielpütz. Magnetic resonance imaging of lung perfusion. *Journal of Magnetic Resonance Imaging*, 59(3):784–796, 2024.

[9] Alexey Voskrebenzev, Martin Gutberlet, Filip Klimeš, Till F. Kaireit, Christian Schönfeld, Anne Rotärmel, Frank Wacker, and Jens Vogel-Claussen. Proton MRI of the lung: How to tame scarce protons and fast signal decay. *Journal of Magnetic Resonance Imaging*, 53(5):1344–1357, 2021.

[10] Catherine Westbrook. *MRI at a Glance*. Wiley-Blackwell, 3 edition, 2016.

[11] Matthew M. Willmering, Ryan K. Robison, Hui Wang, James G. Pipe, and Jason C. Woods. Implementation of the FLORET ultrashort echo-time sequence for lung imaging. *Magnetic Resonance in Medicine*, 82(3):1091–1100, 2019.

[12] Linyu Wu, Chen Gao, Ting Wu, Ning Kong, Ziwei Zhang, Jie Li, Li Fan, and Maosheng Xu. Magnetic resonance imaging in the clinical evaluation of lung disorders: Current status and future prospects. *Journal of Magnetic Resonance Imaging*, 62:1260–1279, 2025.